

Ultrastrong Absorption Meets Ultraweak Absorption: Unraveling the Energy-Dissipative Routes for Dye-Sensitized Upconversion Luminescence

Bin Xue,^{§, ‡} Dan Wang,[§] Langping Tu,^{‡, ||} Dapeng Sun,^{||} Pengtao Jing,[‡] Yulei Chang,[‡] Youlin Zhang,^{ ‡} Xiaomin Liu,[‡] Jing Zuo,^{‡, †, ||} Jun Song,^{* §} Junle Qu,^{* §} Evert Jan Meijer,^{||} Hong Zhang,^{||} and Xianggui Kong^{* ‡}*

[§] Key Lab of Optoelectronics Devices and Systems of Ministry of Education/Guangdong Province, Shenzhen University, 518060 Shenzhen, China

[‡] State Key Laboratory of Luminescence and Applications, Changchun Institute of Optics, Fine Mechanics and Physics, Chinese Academy of Sciences, Changchun 130033, China.

[†] Graduate University of the Chinese Academy of Sciences, Beijing 100049, China

^{||} Van't Hoff Institute for Molecular Sciences, University of Amsterdam, Science Park 904, 1098 XH Amsterdam, The Netherlands.

AUTHOR INFORMATION

Corresponding Author

*E-mail: songjun@szu.edu.cn.; jlqu@szu.edu.cn.

*E-mail: zhangyl@ciomp.ac.cn.; xgkong14@ciomp.ac.cn.

Part I. Materials and Methods.	3
Part II. Supporting data.	8
Part III. Estimation of linked dyes	15
Part IV. FRET radius calculation	16
Part V. Monte Carlo simulation of EM process	17
Part VI. Estimations of the enhanced population rates	30
Part VII. Photobleaching test of dyes	32
Part VIII. References.	33

Part I. Materials and Methods

Materials: IR-780 iodide (99%), 4-mercaptobenzoic acid (99%), $\text{ErCl}_3 \cdot 6\text{H}_2\text{O}$ (99.99%), $\text{YbCl}_3 \cdot 6\text{H}_2\text{O}$ (99.99%), $\text{YCl}_3 \cdot 6\text{H}_2\text{O}$ (99.99%), 1-octadecene(90%)(ODE), oleyamine (90%)(OM) and oleic acid (90%)(OA), were purchased from Sigma-Aldrich. $\text{Y}(\text{CF}_3\text{COO})_3$, $\text{Yb}(\text{CF}_3\text{COO})_3$, CF_3COONa were purchased from GFS Chemicals, NaOH , NH_4F , CH_2Cl_2 , CHCl_3 and were purchased from Beijing Chemical Works, $\text{Nd}(\text{CF}_3\text{COO})_3$ was prepared by dissolving the Nd_2O_3 in excess CF_3COOH and then evaporating CF_3COOH and water completely. All other chemical reagents were of analytical grade and were used directly without further purification.

Procedures for the synthesis of IR-806. The IR-806 was synthesized according to the method described in the literature.¹ IR-780 iodide (250 mg), 4-mercaptobenzoic acid (115.5 mg), and DMF (10 mL) were put in a 50 ml three-neck round bottom flask. The reaction was under N_2 protection for 17 hours. After that, the solution was filtered through a 0.45 μm PTFE syringe filter, and reduced pressure distillation to remove DMF. The residue was dissolved in CH_2Cl_2 (5 mL). The solution also filtered through a 0.45 μm PTFE syringe filter and the final product was precipitate by cool diethyl ether. The products were collected by vacuum filtration, and dried under vacuum. ^1H NMR (500 MHz, CDCl_3) spectrum (Figure S1) showed below, which was also similar to previous report.¹

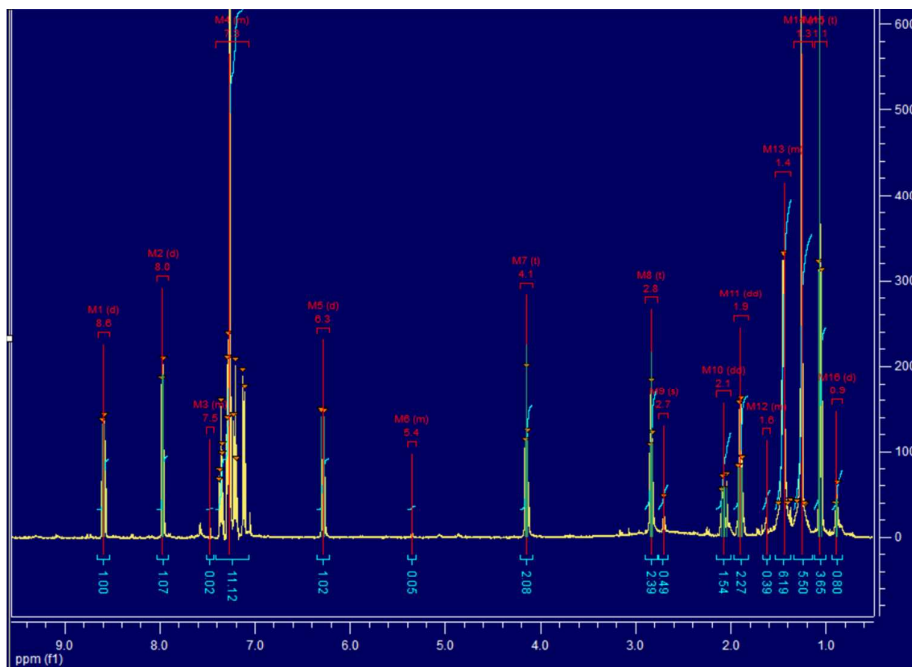


Figure S1. $^1\text{H-NMR}$ (500 MHz, CDCl_3) spectrum of IR-806.

General procedure for synthesis of Nd-shell precursor:

The shell precursor was first prepared according previously reported procedures.²⁻³ In a typical synthesis of $\text{NaYF}_4: \text{Nd}$ ($x\%$) ($x=10\%$, 20% , 40% , 80% , 100%) shell precursor, Neodymium trifluoroacetate precursor $\text{Nd}(\text{CF}_3\text{COO})_3$ ($x=0.1\text{mmol}$, 0.2mmol , 0.4mmol , 0.8mmol , 1.0mmol). Yttrium trifluoroacetate ($1-x$) mmol and Sodium trifluoroacetate (1 mmol) was added to the precursor along with oleic acid (3 mL), oleylamine (3 mL), and 1-octadecene (5 mL) and heated to $120\text{ }^\circ\text{C}$ under vacuum for 45 min to remove residual water and oxygen. The obtained transparent solution was subsequently heated to $290\text{ }^\circ\text{C}$ (under argon and vigorously stirred for 45 min), and then cooled down to room temperature. The resulting nanoparticles were washed with ethanol and finally dispersed in 2 mL ODE .

General procedure for synthesis of $\beta\text{-NaYF}_4: \text{Yb/Er}$ (25/2%) @ $\text{NaYF}_4: \text{Nd}$ (10%)

core-shell nanopaticals:

β -NaYF₄:Yb/Er (25/2%)@NaYF₄:Nd(10%) core-shell nanopaticals were synthesized based on a previously reported procedure according to a previous report with certain modification.² YbCl₃•6H₂O (99.9%) 0.125 mmol, YCl₃•6H₂O (99.9%) 0.365 mmol and ErCl₃.6H₂O(99.9%) 0.01 mmol were dissolved in 3 mL OA, 7.5 mL ODE, and the mixture was heated to 150 °C and kept 30 min, then cool down to room temperature under argon protection. NH₄F (2 mmol), NaOH (1.25 mmol) were dissolved in 5 mL methanol and added to three neck flask. Afterwards, the solution was heated to 70 °C to remove methanol and subsequently heated to 300 °C for 1 hour. After that, 0.5 mmol NaYF₄: Nd (10%) active shell precursor in octadecene was injected into reaction mixture and ripened for 10 min. Finally, the solution was cooled down to room temperature and precipitated by ethanol, centrifuged for three times and finally dispersed in 6 mL CHCl₃.

Synthesis of β -NaYF₄:Yb/Er (25/2%)@NaYF₄:Nd(x%) (x=20%, 40%, 80%, 100%) core-shell nanoparticles:

The nanoparticles with different concentration of Nd³⁺ active-shell was performed exactly as outlined for β -NaYF₄:Yb/Er (25/2%) @ NaYF₄:Nd (10%) nanoparticles mentioned above, except that injected small sacrifice nanoparticles (SNPs, α -NaYF₄:Nd(x%) (x=20%, 40%, 80%, 100%), 0.5 mmol) into a solution of core in epitaxial growth of the larger nanoparticles, respectively.

Conjugating dyes of IR-806 to the surface of core-shell UCNPs

IR-806 can coordinate with UCNPs through the carboxyl group, then the process of IR-806 conjugating on UCNPs is a process of ligand exchange. The nanoparticles had been centrifuged at least three times after preparation to remove the ligands of oleic acid as much as possible. Then 1 mL IR-806 (x mg/mL, $x=0 \sim 20$ mg/mL) in CHCl_3 were mixed with 1 mL $\beta\text{-NaYF}_4\text{:Yb/Er}(25/2\%) @ \text{NaYF}_4\text{:Nd}(20\%)$ nanoparticles (the activator concentration of $\text{Er}^{3+} \sim 1.67$ mM) in CHCl_3 . The reaction mixture was stirred for 24 hours at room temperature, centrifuged and re-dispersed in 1 mL CHCl_3 . And then IR-806 sensitized UCNPs were diluted at least 200 times for luminescence measurement.

General sample characterizations: The transmission electron microscopy (TEM), elemental mapping of the core-shell nanoparticles, line-profile analysis measurement was carried out on a Tecnai G2 F20 S-Twin electron microscopy operating at 200 KV. X-ray diffraction (XRD) measurements were performed with a Rigaku D/max-2000 diffractometer using Cu K α radiation ($\lambda=1.5406$ Å). Absorption spectra were recorded by a Maya 2000 spectrometer (Ocean optics). NIR emission spectra and upconversion luminescence spectra were acquired with FLS980 spectrometer under excitation of 808 nm diode lasers. The quantum yield was measured directly using a Horiba Quanta- ϕ integrating sphere system. The lifetimes of UCNPs were measured with a 500 MHz Tektronix digital oscilloscope model TDS 3052 and excitation light resource generated from an Optical Parametric Oscillator (Sunlite 8000).

Ultrafast TA experiments were conducted using a Ti:sapphire laser (Spectra-Physics, Spitfire ACE, 800 nm, 4.5 mJ/pulse, fwhm 35 fs, 1 kHz), pump pulses at 720 nm were generated by frequency doubling of the fundamental laser in a BBO crystal). Upon femtosecond pulse excitation, a number of electrons in ground state were populated into excited states resulting in the ground-state bleaching (GSB) featured at about 806 nm in TA spectrum (Figure 3b). Then three possible depopulation channels happened: spontaneous emission, stimulated emission (SE), and excited state absorption (ESA), respectively. In general, spontaneous emission cannot be detected in TA spectrum. When the probe pulse passed through the excited volume, the SE process induced a negative feature at around 825 nm in TA spectrum. The GSB peak (~806 nm) and SE peak (~825 nm), overlapped with each other, which contributed to the negative signals. Electrons in the lowest excited states can further absorb probe photons to jump to higher energy levels. Two ESA features (peak at 504 and 575 nm) were observed in Figure 3b.

Part II. Supporting Data.

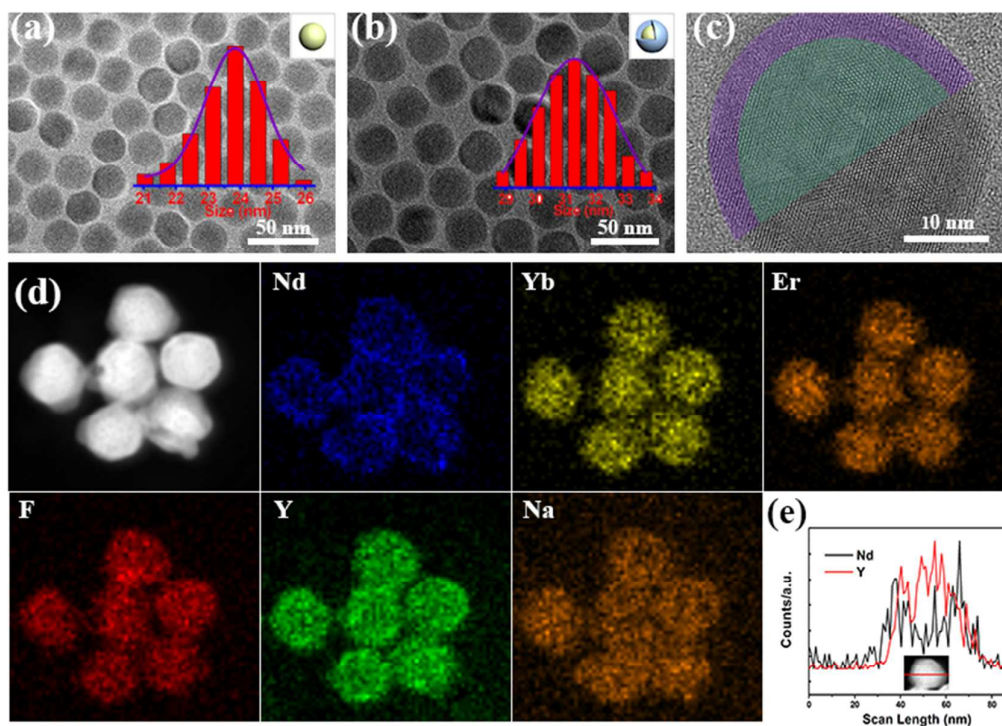


Figure S2. TEM images of (a) NaYF₄:Yb/Er (25/2%) nanoparticles (core, $\sim 23.9 \pm 1.8$ nm) and (b) NaYF₄:Yb/Er (25/2%)@NaYF₄:Nd(20%) nanoparticles (core-shell, $\sim 31.3 \pm 1.1$ nm). (c) HRTEM image of the corresponding core-shell nanoparticles. (d) HAADF-STEM images and elemental mapping of the core-shell nanoparticles. (e) Line-profile analysis (normalization) of the core-shell nanoparticles with Nd, Y lanthanide elements. The increasing size (Figure S2a-S2b), HRTEM (Figure S2c), High angle annular dark-field scanning TEM (HAADF-STEM) (Figure S2d) and line profile elemental analysis (Figure S2e) indicated the successful synthesis of Nd-doped core-shell nanostructures.

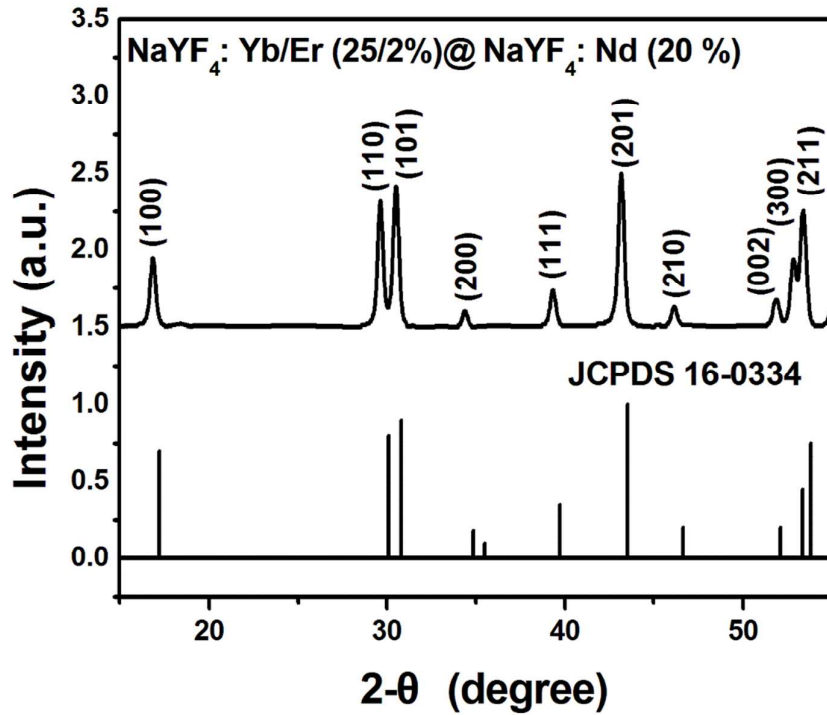


Figure S3. XRD diffraction pattern of the $\text{NaYF}_4:\text{Yb/Er}(25/2\%) @ \text{NaYF}_4:\text{Nd}(20\%)$ nanoparticles and the standard reference pattern $\beta\text{-NaYF}_4$ (JCPDS-16-0334, bottom).

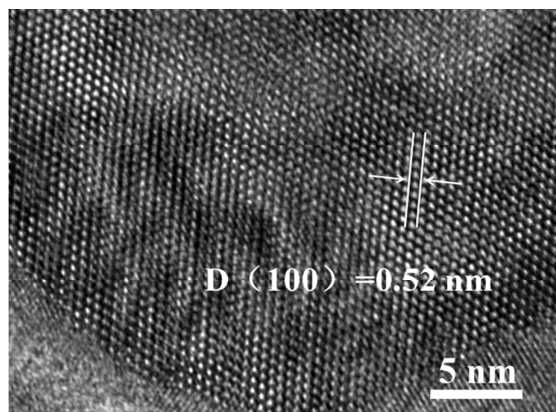


Figure S4. High-resolution TEM (HRTEM) of $\text{NaYF}_4:\text{Yb/Er}(25/2\%) @ \text{NaYF}_4:\text{Nd}(20\%)$ core-shell nanoparticles, the typical d-spacing of ~ 0.52 nm, corresponding to the (100) plane of the hexagonal NaYF_4 phase. Figure S3-S4 demonstrated the

successful synthesis of hexagonal core-shell nanoparticles.

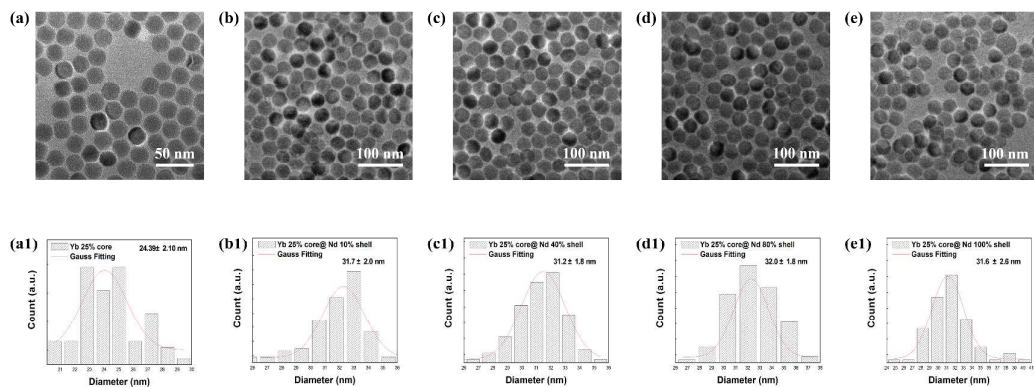


Figure S5. TEM images of other nanoparticles of (a) NaYF₄: Yb/Er (25/2%) nanoparticles, (b) NaYF₄: Yb/Er (25/2%)@ NaYF₄: Nd(10%) nanoparticles, (c) NaYF₄: Yb/Er (25/2%)@ NaYF₄: Nd(40%) nanoparticles, (d) NaYF₄: Yb/Er (25/2%)@ NaYF₄: Nd(80%) nanoparticles, (e) NaYF₄: Yb/Er (25/2%)@ NaYF₄: Nd(100%) nanoparticles. The size distribution of (a1) NaYF₄: Yb/Er (25/2%) nanoparticles, (b1) NaYF₄: Yb/Er (25/2%)@ NaYF₄: Nd(10%) nanoparticles, (c1) NaYF₄: Yb/Er (25/2%)@ NaYF₄: Nd(40%) nanoparticles, (d1) NaYF₄: Yb/Er (25/2%)@ NaYF₄: Nd(80%) nanoparticles, (e1) NaYF₄: Yb/Er (25/2%)@ NaYF₄: Nd(100%) nanoparticles.

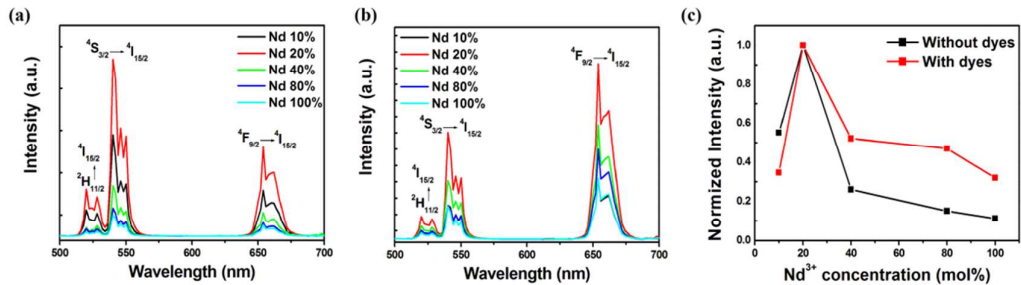


Figure S6. UC emission spectra of NaYF₄: Yb/Er (25/2%)@ NaYF₄: Nd (x%) shell (x=10, 20, 40, 80, 100) nanoparticles without linking dyes (a) and linking with dyes (b), and (c) the corresponding normalized integrated intensity spectra as the function of Nd³⁺ concentration. Though dye-sensitization could not elevate the optimal concentration of Nd³⁺ in our system, the UCL intensity difference has been shortened when doping more Nd³⁺ ions (Figure S6c), which may arise from that doping more Nd³⁺ ions will extract more energy from dyes to UCNPs (Figure 3c), which alleviates the concentration quenching of Nd³⁺. Due to dye-sensitized Nd20 CS owning the strongest UCL, we chose the Nd20 CS as the basic model to discuss the issues in this work.

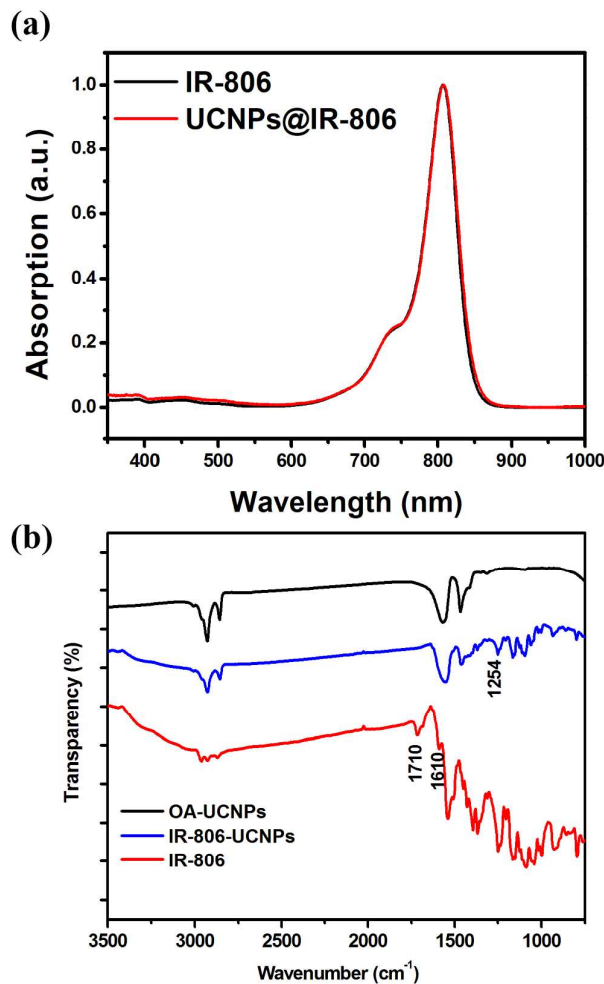


Figure S7. (a) The absorption spectra of IR-806 (black line) and IR-806 coated UCNPs (red line), which demonstrated that the absorption of dyes was nearly unchanged, (b) FT-IR spectra of UCNPs (black line), IR-806 coated UCNPs (blue line), IR-806 (red line). The FTIR spectra in Figure S7b shows that for free IR-806, the C=O stretching vibration mode of the carboxyl group is located between 1610 and 1710 cm^{-1} . After attached on the UCNPs, the vibration modes of the carboxyl group were disappeared and new peaks at $\sim 1254 \text{ cm}^{-1}$ appeared, corresponding to the C-O stretching mode, which meant bond formation between the IR-806 and UCNPs.

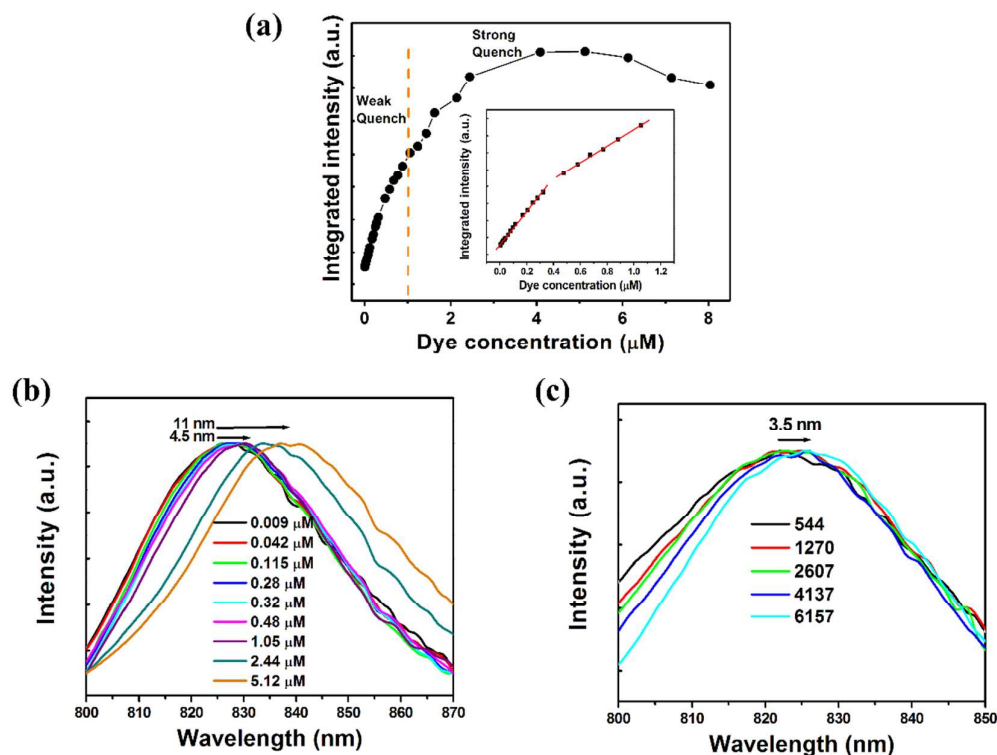


Figure S8. NIR emission intensity integration (a) and normalized NIR emission spectra (b) of free dyes in CHCl_3 solution as the function of dye concentrations. (c)

NIR emission (normalized) of IR-806 sensitized UCNP as a function of the conjugated dye numbers per UCNP. Figure S8a shows that the slope of emission intensity of dyes gradually decreased when the concentration of dyes beyond 0.4 μM , indicating self-quenching or inner filter effects happened. When the self-quenching effects happened, simultaneously, the peak position would be evidently red-shifted (Figure S8b). Whereas, the slight drop of the slope of NIR emission (Figure 2a and the little red-shifted peak position (Figure S8c), which suggest only a little self-quenching effect happened.

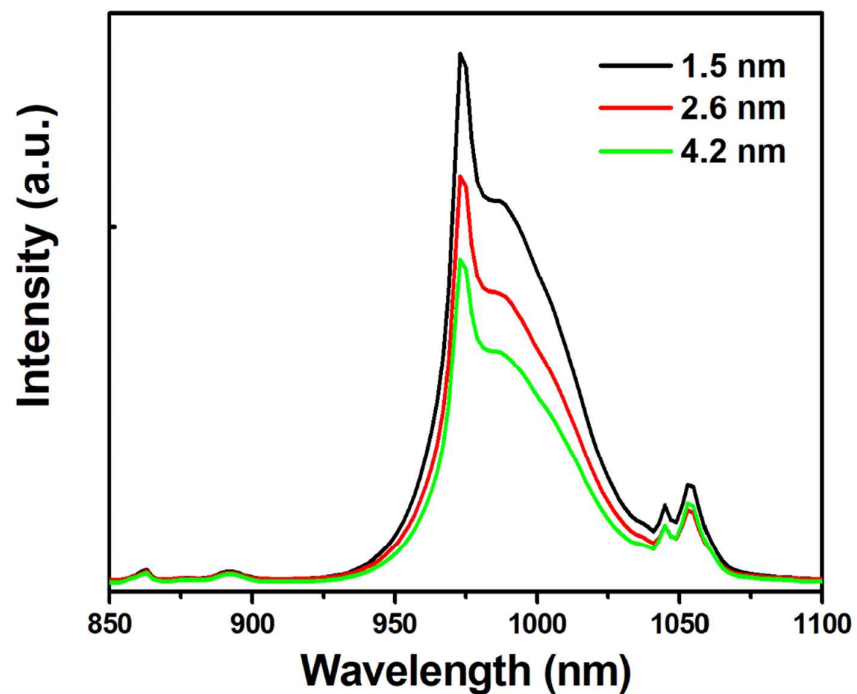


Figure S9. NIR emissions of Yb³⁺ of core@Nd-doped shell@inert shell (CSS) nanoparticles with different Nd-shell thickness of 1.5 nm, 2.6 nm, 4.2 nm. The NIR emissions were normalized to their absorption of Nd³⁺ ions. These CSS samples with different thickness of Nd-doped shell were obtained from our previous work.²

Part III. Estimation of linked dyes

Estimations of Number of Dyes per Core-Shell UCNPs

The NaYF₄: Yb/Er (25/2%)@ NaYF₄: Nd(20%) UCNPs have a core size of 23.9 nm core and a core-shell size of 31.3 nm.

For the fomular weight of core NaYF₄: 25%Yb, 2%Er, $M_{\text{core}}=210.5$

$$\text{NaYF}_4: 25\% \text{Yb}, 2\% \text{Er} = 23 + 19 \times 4 + (88.9 \times 0.73 + 173.05 \times 0.25 + 167.26 \times 0.02) = 99 + (64.9 + 43.26 + 3.35) = 210.5$$

For the fomular weight of shell NaYF₄:20%Nd, $M_{\text{shell}} = 23 + 19 \times 4 + (88.9 \times 0.8 + 144.24 \times 0.2) = 198.97$

$$V_{\text{core}} = 4\pi r_{\text{core}}^3 / 3 = 4 \times 3.14 \times (23.9/2)^3 / 3 = 4 \times 3.14 \times 1622/3 \text{ nm}^3 = 7145 \text{ nm}^3$$

$$V_{\text{shell}} = 4\pi r_{\text{shell}}^3 / 3 - 4\pi r_{\text{core}}^3 / 3 = 4 \times 3.14 \times (31.3/2)^3 / 3 - 7145 = 16048 - 7145 = 8903 \text{ nm}^3$$

$$V = 16048 \text{ nm}^3$$

$$M_{\text{average}} = (V_{\text{core}}/V)M_{\text{core}} + (V_{\text{shell}}/V)M_{\text{shell}}$$

$$= 7145/16048 \times 210.5 + 8903/16048 \times 198.97 = 93.7 + 110.4 = 204.1$$

$$a = 5.96 \text{ \AA}, c = 3.53 \text{ \AA},$$

$$V_{\text{cell}} = \sqrt{3}/2 \times a^2 c = 108.6 \text{ \AA}^3$$

The mass of single UCNP is:

$$m_{\text{NP}} = 1.5 M_{\text{average}} \cdot V / N_{\text{A}} \cdot V_{\text{cell}} = 1.5 \times 222.5 \times 16048 \times 10^3 / (6.02 \times 10^{23} \times 108.6) = 8.19 \times 10^{-17} \text{ g}$$

Therefore, the number of UCNPs is calculated from the test weight of UCNPs:

$$N_{\text{UCNPs}} = m_{\text{UCNPs}} / m_{\text{NP}} = 9.76 \times 10^{13}$$

The number of IR-806 is determined by absorption :

$$N_{\text{IR-806}} = (A/\epsilon_{\text{IR-806}} \times l) \times V_{\text{test}} \times N_{\text{A}} = 2.54 \times 10^{17}$$

The number of IR-806 dye per UCNPs is given:

$$N_{\text{per dye}} = (N_{\text{IR-806}}) / (N_{\text{UCNPs}}) = 2602$$

Part IV. FRET Radius Calculation

The Förster distance or Förster radius R_0 is defined as:⁴

$$R_0^6 = \frac{9 \ln(10)}{128 \pi^5} \times \frac{\Phi_D \kappa^2 J}{n_D^4 N_A} \quad (\text{S1})$$

where Φ_D is the quantum yield of the donor, κ is dipole orientation factor (here $\kappa^2 = 2/3$ typically for randomly oriented systems), n_D is the refractive index of the measuring medium ((here $n_D = 1.489$), N_A is the Avogadro number, J is the overlap integral, which defined as:

$$J = \int_0^\infty I_D(\lambda) \varepsilon_A(\lambda) \lambda^4 d\lambda \quad (\text{S2})$$

where I_D and ε_A represent the donor area-normalized emission spectrum and acceptor molar absorptivity (or extinction coefficient) spectrum, respectively.

According to Eq. (S1), we can see that, the Förster radius R_0 is determined by the quantum yield Φ_D and the overlap integral J . In our system, the quantum yield Φ_D of the dyes was tested about 1.74%, $J_{\text{dye-UCNPs}}$ is calculated to be $6.35 \times 10^{11} \text{ nm}^4 \text{ M}^{-1} \text{ cm}^{-1}$, the Förster radius $R_{0\text{ET}}$ is estimated about 0.75 nm.

Part V. Monte Carlo simulation of EM process

1. Basic picture of simulation model.

Similar to our previous work,⁵ we established a Monte Carlo simulation model (a three-dimensional random walk of excited states in the sublattice) to study the energy migration on the core-shell interface of heterogeneous nanostructures. We calculated the final percent of excitation energy from the outside shell into the inner core when varying the thickness of the Nd-doped layer. The calculations include three cases below:

(1) without surface quenching effects, the Nd^{3+} ions in the Nd-doped layer are uniformly excited, the calculation results are shown in Figure 4a.

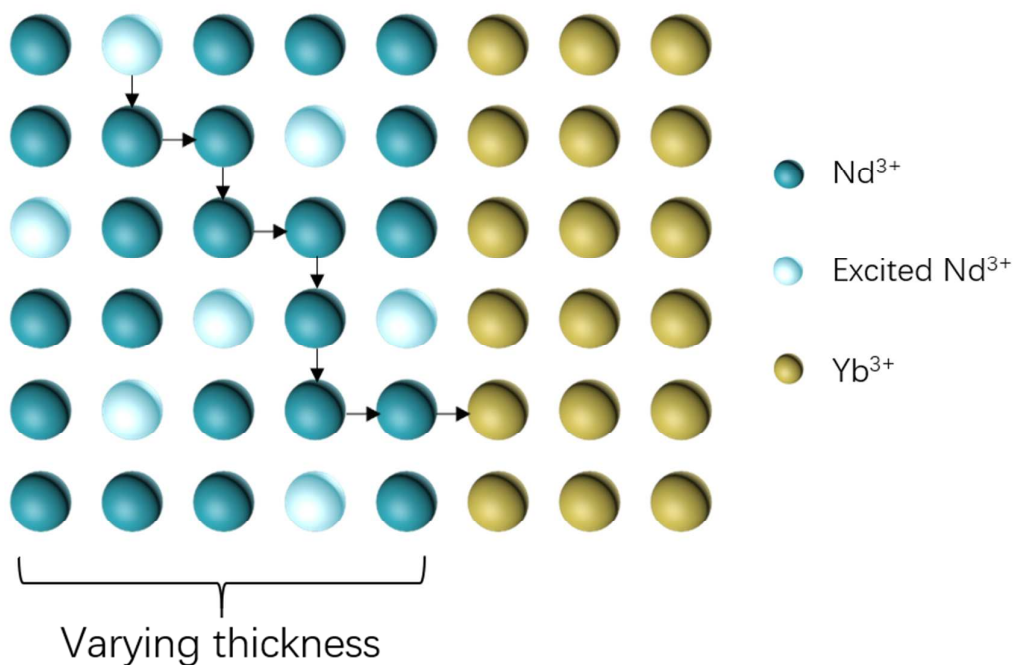


Figure S10. Schematic diagram of the microscopic picture of EM process.

(2) the Nd^{3+} ions in the Nd-doped layer are uniformly excited, the calculation results are shown in Figure 4c left.

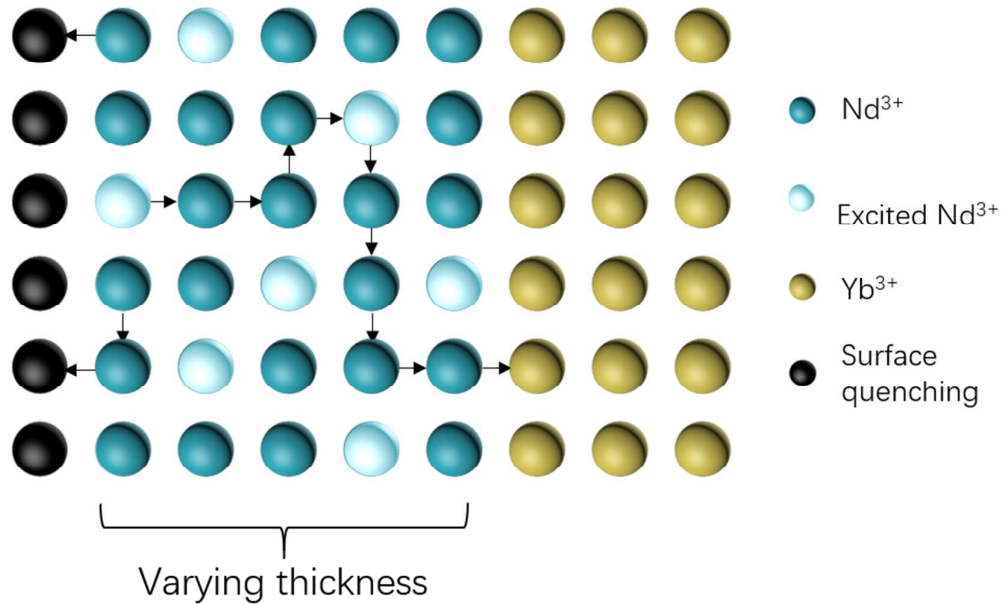


Figure S11. Schematic diagram of the microscopic picture of EM process.

(3) the Nd^{3+} ions in the outmost layer of the Nd-doped layer are excited and the surface quenching effects are considered, the calculation results are shown in Figure 4c right.

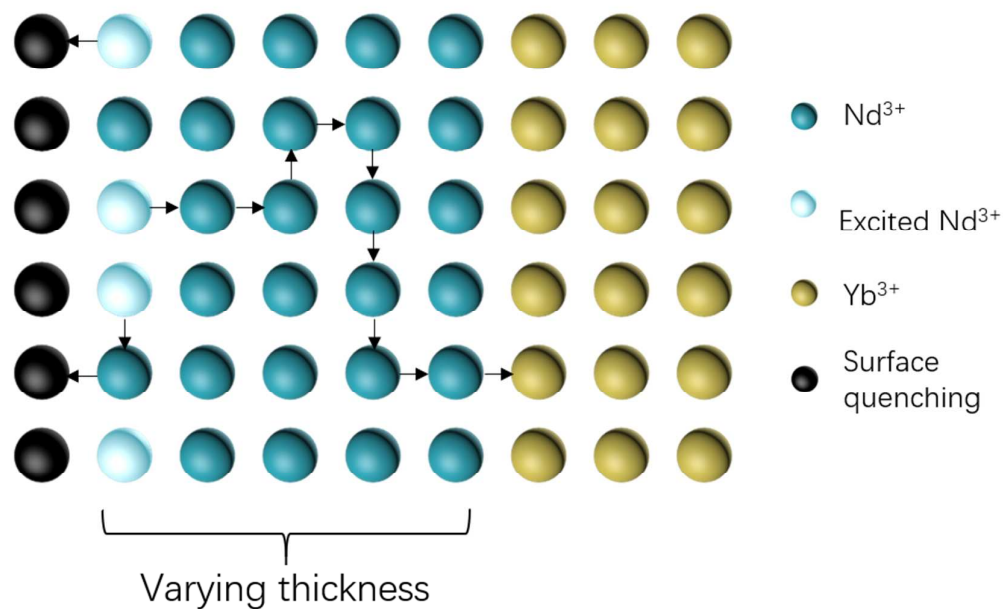


Figure S12. Schematic diagram of the microscopic picture of EM process.

2. Construction of simulation model.

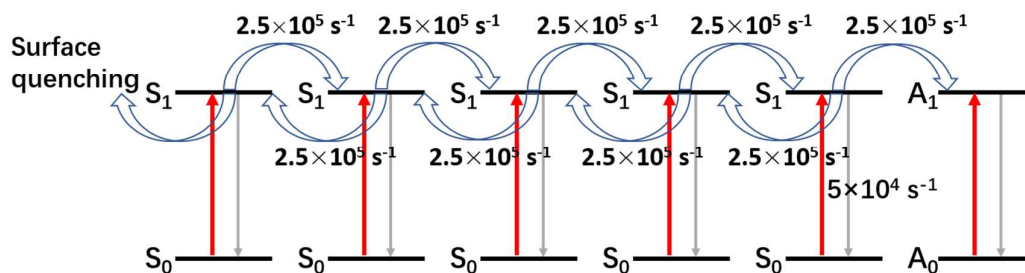


Figure S13. The Monte Carlo simulation model of energy migration processes in the Nd-doped core-shell nanostructure. $S_{0,l}$ and $A_{0,l}$ are the simplified energy levels of sensitizer (Nd^{3+}) and acceptor (Yb^{3+}), respectively.

Table S1. The parameters used in the simulations.

<i>Parameters</i>	<i>Value</i>
Simulation time period (s)	3
Time step (s)	10^{-6}
Recombination rate of S_1 (s^{-1}) ^a	$5 \times 10^4 s^{-1}$
Energy migration rate from $S_1 \rightarrow S_0$ (s^{-1}) ^{b,c}	$2.5 \times 10^5 s^{-1}$
Energy transfer rate from $S_1 \rightarrow A_0$ (s^{-1}) ^c	$2.5 \times 10^5 s^{-1}$
Absorption cross-section of S_0 (cm^2) ^d	1.2×10^{-19}
Surface quenching rate (s^{-1}) ^c	$2.5 \times 10^5 s^{-1}$

^a From Zuo *et al.*⁵

^b From Lupei *et al.*⁶

^c Estimated below.

^d From Wang *et al.*⁷

The energy migration rate of Nd^{3+} is a key parameter, which is difficult to obtain. Lupei *et al.*⁶ gave a estimated migration parameter $\sim 450 s^{-1} (x \%)^2$ (x is the concentration range from 1–10 at% Nd), therefore, in our case, for NaYF₄: Nd(20%) UCNP, the energy migration rate of Nd^{3+} should be estimated to 10^5 – $10^6 s^{-1}$. We applied the simulation at different migration rates ($1.5 \times 10^5 s^{-1}$, $2.5 \times 10^5 s^{-1}$, $5 \times 10^5 s^{-1}$, $1 \times 10^6 s^{-1}$, $2.5 \times 10^6 s^{-1}$, $5 \times 10^6 s^{-1}$). We chose $2.5 \times 10^5 s^{-1}$ as the basic migration rate of Nd^{3+} , which is also closed to the estimated value of Lupei *et al.*⁶ Actually, the other migration rates also obtain the similar qualitative calculation results (Figure S15-S20),

which show the same trend in Figure 4. Similar to our previous work, we also assumed that surface quenching rate equals to the energy migration rate of Nd^{3+} . The simulation model stops when excitation energy passes through the interface into the inner core, then we assumed the energy transfer rate from Nd^{3+} to Yb^{3+} ($S_1 \rightarrow A_0$) equals to the energy migration rate of Nd^{3+} .

Similarly, as a proof of concept simulation, some reasonable simplifications are considered in this work:

1: The construction of the nanostructure: the simple cubic lattice is chosen to simplify the crystal structure of the nanostructure. According to the Nd^{3+} doping concentration and the lattice parameters of hexagonal phase NaYF_4 matrix, the calculated distance between the nearest neighboring ions is about 0.8 nm. Accordingly, the 24 nm core is coated with 2, 3 and 5 layers of Nd^{3+} ions (corresponding to 1.6 nm, 2.4 nm and 4 nm thickness of the Nd-doped shell).

2: The energy states of Nd^{3+} and Yb^{3+} are shown in Figure S13. The energy levels of Nd^{3+} ions have two energy levels (labeled as S_1 and S_0 , respectively), which are reasonably simplified without affecting the basic understanding of the model.

3: The number of excited states is chosen to keep 5 %, which is beneficial to make sure all the calculation processes can finish in time and to obtain the stable statistics output results.

4: The energy transfer/migration processes only occur between the two closest neighboring ions.

3. Simulation approach

Based on the fixed parameters and the simulation model, the simulation approach is performed based on our previous work.⁵ We tracked time evolution of the excited states (distributed in the overall Nd-doped layer or in the outmost layer of the Nd-doped layer) in the system. For every excited ion, we calculated its microscopic probabilities at each time step for the following processes: a) energy transfer, b) energy migration, c) recombination to the ground state d) surface quenching (when the surface quenching sites are located on the nanoparticle surface). And the probabilities of each event is:

$$P_i = R_i \Delta t \quad (\text{S3})$$

where R_i is the rates of the each event (shown in Table S1), Δt is the time step (1 μ s) in this work.

In summary, the similar algorithm flowchart of steady-state Monte Carlo simulation is shown in Figure S14.

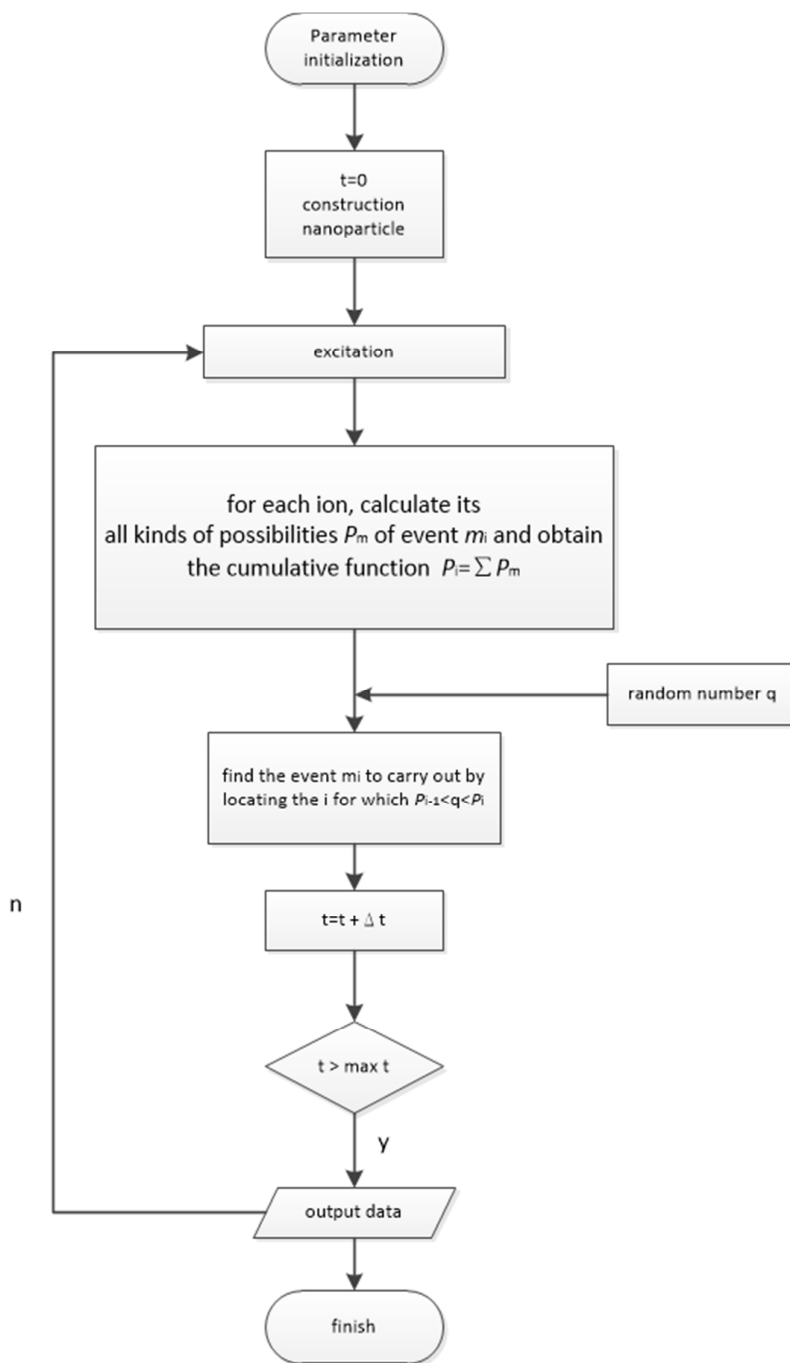


Figure S14. The algorithm flowchart of the Monte Carlo simulation.

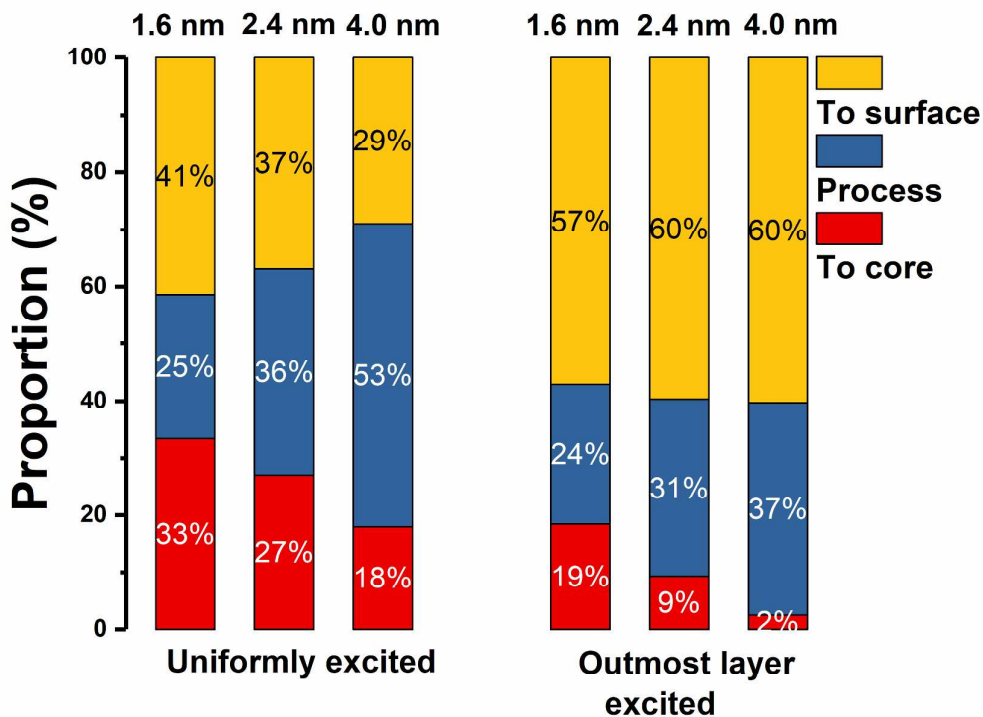


Figure S15. The energy migration rate of Nd^{3+} was set $1.5 \times 10^5 \text{ s}^{-1}$ to perform simulation and the according simulation results, the proportion of excitation energy migrating to surface quenching sites (yellow colour), EM loss during the process of excitation energy passes through the Nd-doped layer (slate blue colour) and the final excitation energy migrating to inner core (red colour) when the Nd-doped layer are uniformly excited (left) and only the Nd^{3+} ions in the outmost layer were excited (right).

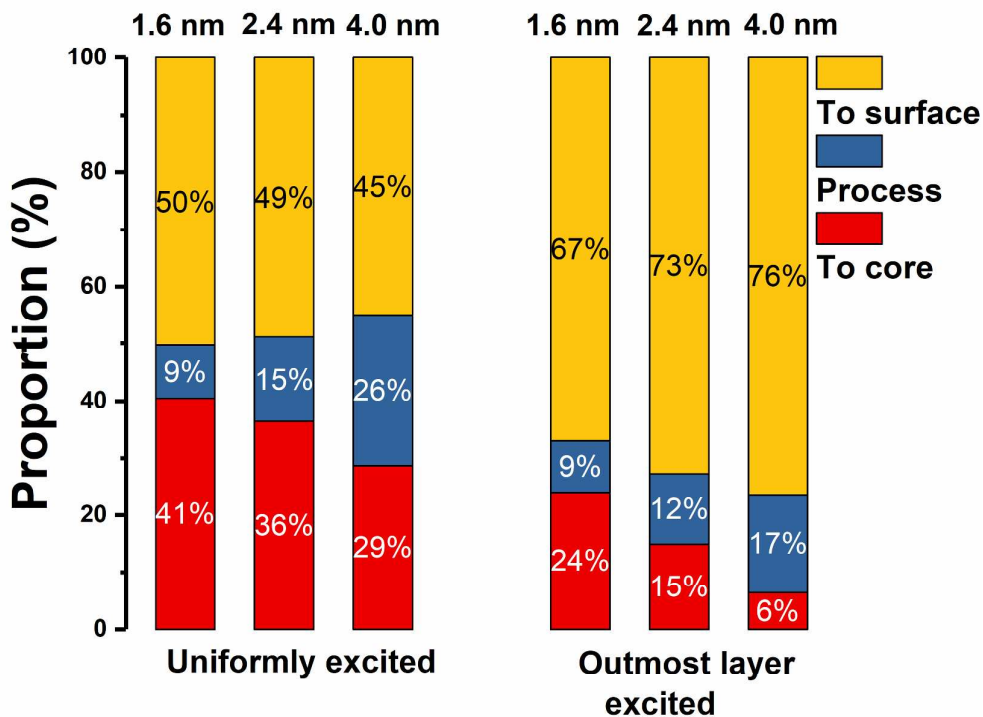


Figure S16. The energy migration rate of Nd^{3+} was set $5 \times 10^5 \text{ s}^{-1}$ to perform simulation and the according simulation results, the proportion of excitation energy migrating to surface quenching sites (yellow colour), EM loss during the process of excitation energy passes through the Nd-doped layer (slate blue colour) and the final excitation energy migrating to inner core (red colour) when the Nd-doped layer are uniformly excited (left) and only the Nd^{3+} ions in the outmost layer were excited (right).

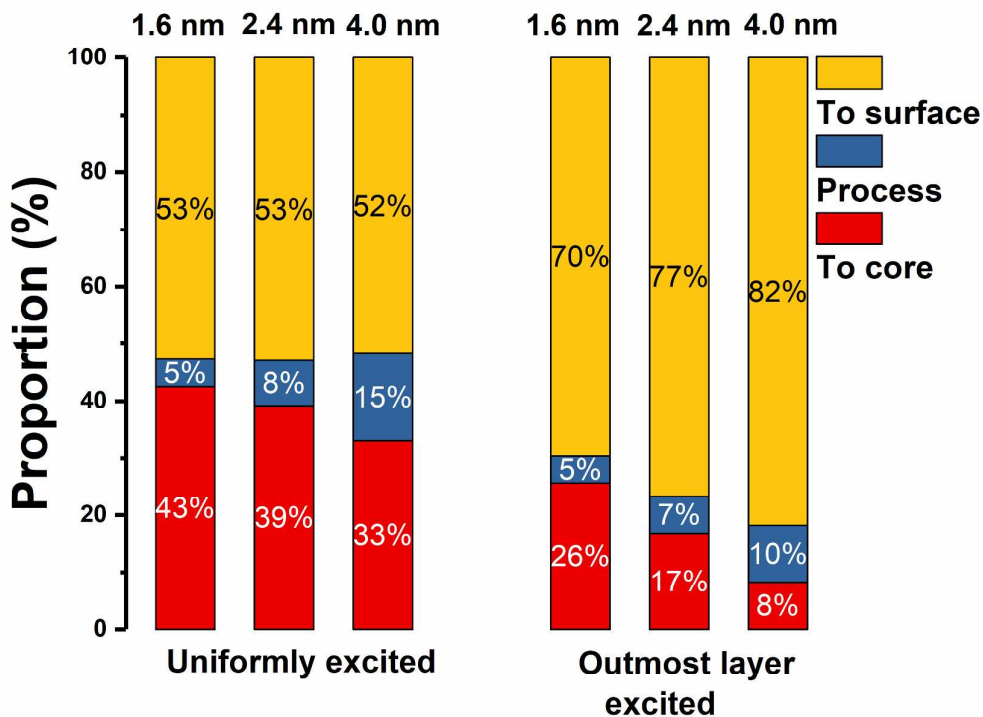


Figure S17. The energy migration rate of Nd^{3+} was set $1 \times 10^6 \text{ s}^{-1}$ to perform simulation and the according simulation results, the proportion of excitation energy migrating to surface quenching sites (yellow colour), EM loss during the process of excitation energy passes through the Nd-doped layer (slate blue colour) and the final excitation energy migrating to inner core (red colour) when the Nd-doped layer are uniformly excited (left) and only the Nd^{3+} ions in the outmost layer were excited (right).

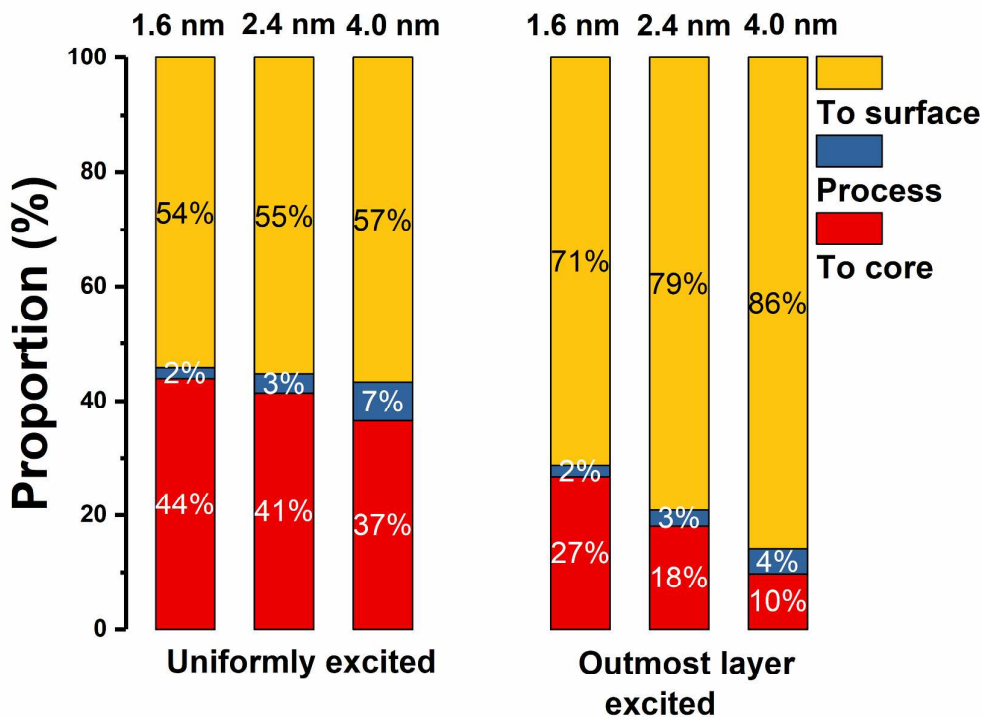


Figure S18. The energy migration rate of Nd^{3+} was set $2.5 \times 10^6 \text{ s}^{-1}$ to perform simulation and the according simulation results, the proportion of excitation energy migrating to surface quenching sites (yellow colour), EM loss during the process of excitation energy passes through the Nd-doped layer (slate blue colour) and the final excitation energy migrating to inner core (red colour) when the Nd-doped layer are uniformly excited (left) and only the Nd^{3+} ions in the outmost layer were excited (right).

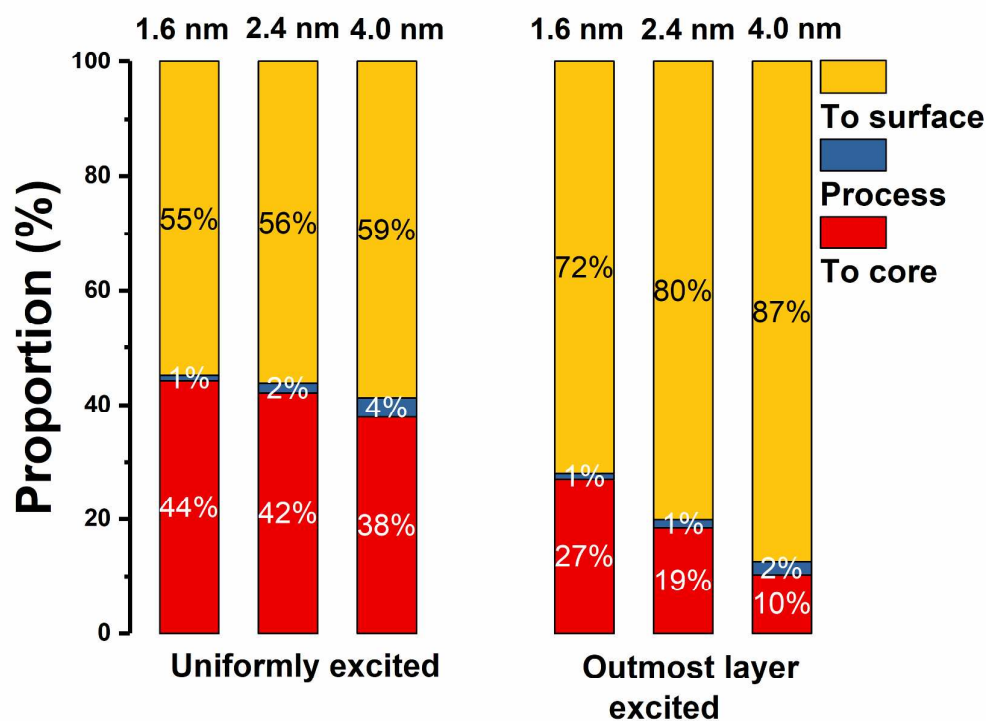


Figure S19. The energy migration rate of Nd^{3+} was set $5 \times 10^6 \text{ s}^{-1}$ to perform simulation and the according simulation results, the proportion of excitation energy migrating to surface quenching sites (yellow colour), EM loss during the process of excitation energy passes through the Nd-doped layer (slate blue colour) and the final excitation energy migrating to inner core (red colour) when the Nd-doped layer are uniformly excited (left) and only the Nd^{3+} ions in the outmost layer were excited (right).

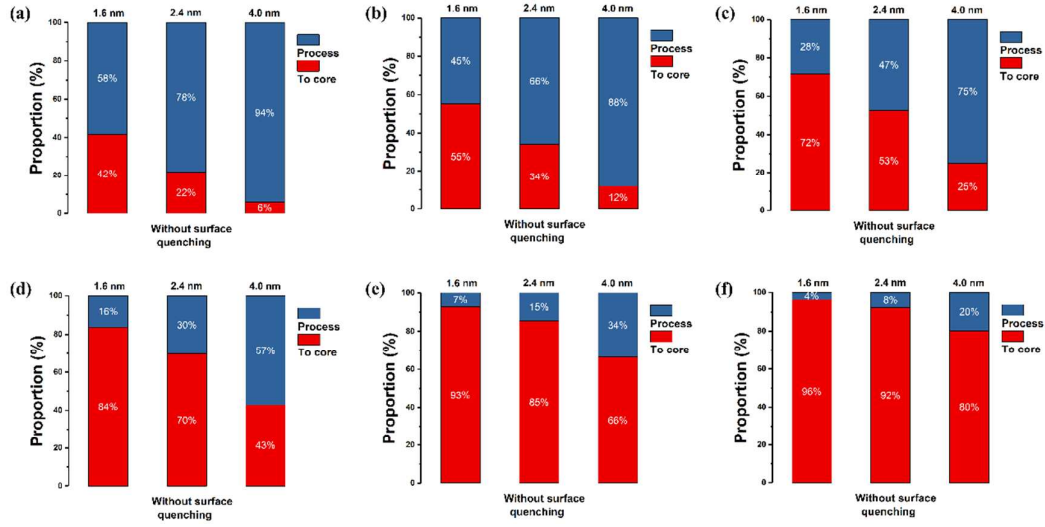


Figure S20. Perform simulations without existing surface quenching, at different migration rates of Nd^{3+} , (a) $1.5 \times 10^5 \text{ s}^{-1}$, (b) $2.5 \times 10^5 \text{ s}^{-1}$, (c) $5 \times 10^5 \text{ s}^{-1}$, (d) $1 \times 10^6 \text{ s}^{-1}$, (e) $2.5 \times 10^6 \text{ s}^{-1}$, (f) $5 \times 10^6 \text{ s}^{-1}$. the proportion of EM loss during the process of excitation energy passes through the Nd-doped layer (slate blue colour) and the final excitation energy migrating to inner core (red colour).

Part VI. Estimations of the Enhanced Population Rates

The population rates of one UCNPs (W_{ex}) can be expressed as:

$$W_{ex} = \rho\sigma_{Nd}N_{per Nd} \quad (S4)$$

where ρ is the excitation photon flux, which is linearly related to excitation power densities, σ_{Nd} is the absorption cross-section of Nd^{3+} , $N_{per Nd}$ is the average number of Nd^{3+} per UCNPs

When UCNPs conjugated with dyes, the population rates of W_{ex}' become:

$$W_{ex}' = (\rho\sigma_{Nd}N_{per Nd} + \rho\sigma_{dye}\eta_{ET}N_{per dye})(1 - \eta_{EBT})(1 - \eta_{EM}) \quad (S5)$$

where σ_{dye} is the absorption cross-section of IR-806, $N_{per dye}$ is the average number of IR-806 per UCNPs, η_{ET} represents the energy transfer efficiency from dyes to UCNPs, η_{EBT} represents the energy transfer efficiency from UCNPs to dyes, η_{EM} represent the EM loss efficiency during the migration process.

According to EQ. (S4)~(S5), the population rates are enhanced as

$$\begin{aligned} P_{EF} &= \frac{W_{ex}'}{W_{ex}} = \frac{(\rho\sigma_{Nd}N_{per Nd} + \rho\sigma_{dye}\eta_{ET}N_{per dye})(1 - \eta_{EBT})(1 - \eta_{EM})}{\rho\sigma_{Nd}N_{per Nd}} \\ &= (1 + A_{EF}\eta_{ET})(1 - \eta_{EBT})(1 - \eta_{EM}) \end{aligned}$$

where A_{EF} is the enhanced factor of the absorption of UCNPs by dye-sensitization, A_{EF} is expressed as:

$$A_{EF} = \frac{\sigma_{dye}N_{per dye}}{\sigma_{Nd}N_{per Nd}} \quad (S6)$$

According to the increase of absorption after dye-sensitization in Figure 2e, A_{EF} was approximated to ~978, η_{ET} was ~ 6.4 % according Figure 3c, η_{EBT} was ~32% when the linked dye numbers per UCNPs was ~2600 according to Figure 4b. According to the

experimental and simulation results (Figure 4), η_{EM} was estimated ~70–95%. Here,

we adopt that η_{EM} is 85%, then the population rates are enhanced as:

$$P_{EF} = \frac{W_{ex}'}{W_{ex}} = (1 + 978 * 0.064)(1 - 0.32)(1 - 0.85) = 6.5$$

Then, the UCL should be approximatively enhanced about $(P_{EF})^2 = 42.3$

Part VII. Photobleaching test of dyes

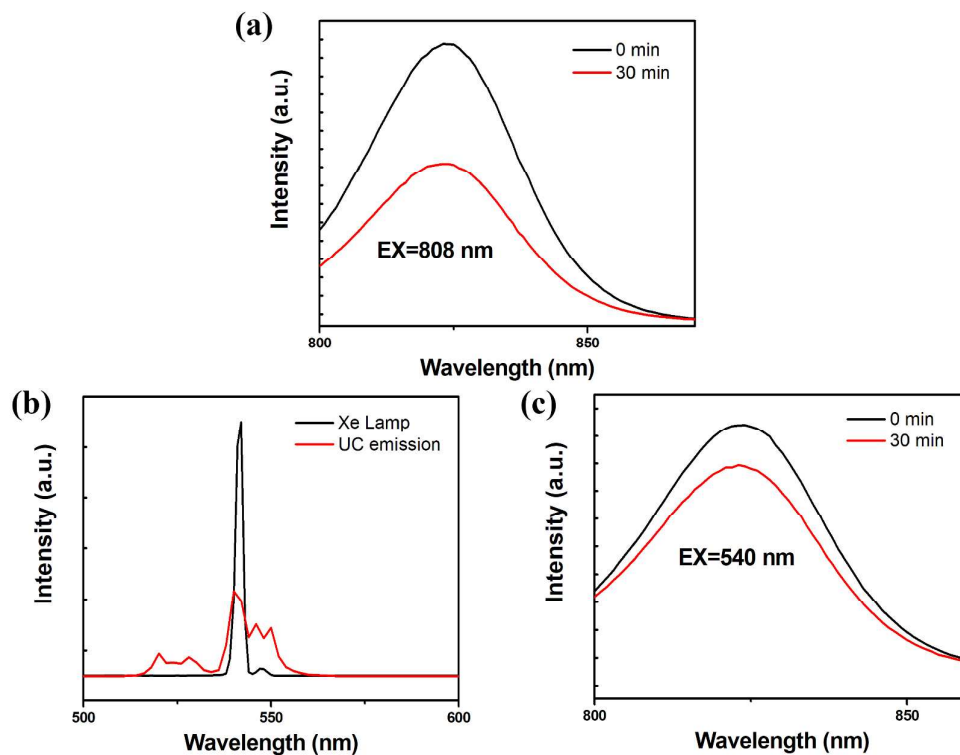


Figure S21. (a) Photobleaching test of dyes by using 808 nm laser (0.12 W) for 30 min. We used the Xe Lamp (~540 nm) with the similar light intensity of green UC emissions (b) irradiating dyes of IR-806 for 30 min to generate the photobleaching results (c).

Part VIII. References

- (1) Zou, W. Q.; Visser, C.; Maduro, J. A.; Pshenichnikov, M. S.; Hummelen, J. C. Broadband dye-sensitized upconversion of near-infrared light. *Nat. Photonics* **2012**, *6* (8), 560-564.
- (2) Wang, D.; Xue, B.; Kong, X. G.; Tu, L. P.; Liu, X. M.; Zhang, Y. L.; Chang, Y. L.; Luo, Y. S.; Zhao, H. Y.; Zhang, H. 808 nm driven Nd³⁺-sensitized upconversion nanostructures for photodynamic therapy and simultaneous fluorescence imaging. *Nanoscale* **2015**, *7* (1), 190-197.
- (3) Johnson, N. J.; Korinek, A.; Dong, C.; van Veggel, F. C. Self-Focusing by Ostwald Ripening: A Strategy for Layer-by-Layer Epitaxial Growth on Upconverting Nanocrystals. *J. Am. Chem. Soc.* **2012**, *134* (27), 11068-11071.
- (4) Lakowicz, J. R. *Principles of fluorescence spectroscopy*. Springer: 2007.
- (5) Zuo, J.; Sun, D. P.; Tu, L. P.; Wu, Y. N.; Cao, Y. H.; Xue, B.; Zhang, Y. L.; Chang, Y. L.; Liu, X. M.; Kong, X. G.; et al. Precisely Tailoring Upconversion Dynamics via Energy Migration in Core-Shell Nanostructures. *Angew. Chem. Int. Ed.* **2018**, *57* (12), 3054-3058.
- (6) Lupei, A.; Lupei, V.; Taira, T.; Sato, Y.; Ikesue, A.; Gheorghe, C. Energy transfer processes of Nd³⁺ in Y₂O₃ ceramic. *J. Lumin.* **2003**, *102*, 72-76.
- (7) Wang, Y. F.; Liu, G. Y.; Sun, L. D.; Xiao, J. W.; Zhou, J. C.; Yan, C. H. Nd³⁺-Sensitized Upconversion Nanophosphors: Efficient In Vivo Bioimaging Probes with Minimized Heating Effect. *ACS Nano* **2013**, *7* (8), 7200-7206.